11

Spectro-Microscopic Study of Laser-Modified Carbon Nanotubes

Cheng-Hao Chuang[1], Chorng-Haur Sow[2] and Minn-Tsong Lin[3*]

[1,3]*Department of Physics, National Taiwan University, Taipei*
[2]*Department of Physics, National University of Singapore*
[3]*Institute of Atomic and Molecular Sciences, Academia Sinica, Taipei*
[1,3]*Taiwan*
[2]*Singapore*

1. Introduction

In 1991, Iijima discovered the needle-like tubes insides the fullerene production through the arc-discharge evaporation method.(1) Using transmission electron microscopy (TEM), a new type of the coaxial tube, namely carbon nanotube (CNT), was observed for the first time. One-dimensional (1D) CNTs are rolled graphitic sheet with a few nanometer in diameter. The other groups demonstrated that it is possible to generate different graphitic layers axially, such as single-wall CNTs (SWCNTs), double-wall CNTs (DWCNTs), and multi-wall CNTs (MWCNTs).(2) The electronic property of these CNTs was observed to be either metallic or semiconducting.(3) As a result, scientists have devoted much attention to study the intrinsic property of different rolled models.(4)

In the case of chemical environment, the sp^2-hybridized carbon sheet establishes the strongly covalent C-C bond, resulting in a high mechanical strength 100 times than that of steel.(5) The outstanding mechanical property is suitable for the tip of atomic force microscopy (AFM).(6) Besides, the chemical inertness built by the stable C-C bond leads to a perfect honeycomb structure with very few defect and gas adsorption. Only a few percentage of gas adsorption gives rise to the huge change of electronic transport property on CNTs surface. Different sensitivities of transportation with various gas species are very useful to identify for gas sensor applications.(7) The large surface area and its hollow interior lead to the potential application in the hydrogen-stored battery utilization. For the advantage of recyclable ability and the enhancement of metallic particles, CNTs is an extremely valuable for energy storage.(8) Besides, it is important for nano-electric devices due to its superior thermal conductivity (6000 W $m^{-1}K^{-1}$ > diamond) and current capacity (10^9 A/cm^2 100 times than that of copper wire).(9) Despite of these exceptional characteristics, it is hard to produce a specific type of CNTs and manipulate its electronic structure to fit the diverse requirements. Therefore, the chemical functionalization route that links the specific chemical group to the tubular surface for its chemical and mechanical tuning offers an attractive post-synthesis technique to tailor the properties of the CNTs to suit the applications. In other words, it offers the functions of CNTs base multiplied by a new potential performance as an integrated device.(10) The types

*mtlin@phys.ntu.edu.tw

of chemical modification are divided into the physisorption and chemisorption on the surface or at the defective site.(11) Owing to the weak interaction between the molecule species and the π-conjugate surface of CNTs, the physisorption method to control electronic structure is not suitable for the exceedingly environmental demand. On the other hand, chemisorbed molecules attach on the surface randomly and thus not assign to the desirable active position for effective hybrid utilization.

In terms of the chemical modification in field emission experiments, plasma effect,(12) heat process,(13) and laser effect(14) are found to be effective methods to improve its emission performance. This is attributed mostly to chemical doping and morphological change. However, detailed knowledge of its local electronic structure remains unknown. Recently, a focused laser system has been developed to trim the CNTs arrays to form three-dimensional structure.(15; 16) After trimming the CNTs array by focused laser, the turn-on electric field decreases and its emission current density increases in a field emission experiment.(14) However, the correlation between laser irradiation and electronic structure of CNTs has not been discussed. Researchers found the larger electron density of state (DOS) at tips of CNTs, which is attributed to the influences of lattice defect, deformed carbon cage, or dangling bond.(17; 18) The sufficient valence electrons at tips plus a strong elasticity, hence, could play an important role in the field emission performance.(19) The electron beam from the tips is more stable and efficient than the other emission systems.

In this work, we present a technique that facilitates exclusive chemical modification of the CNTs with controlled locality using a focused laser beam. With focused laser beam, we can achieve morphological modification and structural rearrangment of the CNTs. With the CNTs housed in a transparent chamber with controlled gaseous environment, we can select the appropriate gas species for the chemical modification. In addition of gas species selection, it can broaden the CNT-based application by choosing chemical bonding species. The electronic structure and its chemical modification of CNTs are suitable to be resolved by X-ray photoelectron spectroscopy (XPS). Due to the localized surface functionalization, Scanning PhotoElectron Microscopy (SPEM) equipped with XPS provides the chemical and elemental information with the spatial resolution of 100 nm. The precise information of electronic structure is investigated by micro-XPS and converted to a mapping image for the spatially resolved chemical analysis by SPEM.(20; 21)The enhanced chemical shift of 0.9 eV in C 1s state is found in the air-treated CNTs. The chemical modifications of nitrogen-treated and oxygen-treated CNTs reveal the less up-shift of C 1s state by 0.6 and 0.2 eV, respectively. In nitrogen-treated and oxygen-treated CNTs, the appearance of C-N (C-O) bond and surface-adsorbed nitrogen (oxygen) gas are both observed on the top area of CNTs. The presence of chemisorbed gas atoms accounts for the origin of up-shift of C 1s state in N_2 and O_2-treated CNTs. Furthermore the chemical shifts dependent on different gaseous environments shall involve the combination of structural defect and the mixing gas molecules. VB spectrum in air-treated CNTs exhibits the DOS transition from the mixing of C 2s and C 2s/2p-σ band to C 2p-π band, which is driven by laser irradiation. In the case of nitrogen-treated (oxygen-treated) CNTs, the spectral features of N 2s (O 2s) band in VB spectra are attributed to the appearance of C-N (C-O) chemical bond of N 1s (O 1s) state. In terms of physisorbed gas contribution, the surface-adsorbed nitrogen molecules in as-grown CNTs bring about a larger rearrangement of DOS than the consequence of nitrogen-treated CNTs. However, in oxygen-treated CNTs, laser irradiation induces the same tendency of DOS transition, which is consistent with the behavior of the air-treated CNTs. By controlling gas molecule species and laser beam, we can modify the chemical composition of CNTs at the

specific region effectively. Our findings will open up a new field of the tuneable electronic structure for the advanced nano-electric applications.

2. CNTs fabrication and its chemical modifications: A new way to add mulitfunctional properties of CNTs

2.1 CNTs fabrication

MWCNTs and SWCNTs can be synthesized by high pressure arc discharge method, laser ablation, or chemical vapor deposition (CVD).(1; 22–24) Our MWCNTs sample is grown on Si substrate by plasma-enhanced CVD (PECVD).(25) After thin SiO_2 layer on Si sample is cleaned, Fe layer is deposited on flesh Si sample by the means of radio frequency magnetron sputtering. In the PECVD chamber, the resistance heating plate is used to raise the temperature of Fe/Si specimen up to 750 °C. The mixture of C_2H_2 and H_2 gas with the flow rate of 15 sccm (standard cubic centimeters per minute) and 60 sccm respectively are introduced into the PECVD chamber. These species are the reactive carbon sources for the construction of CNTs synthesis. The high annealing temperature causes the surface tension of Fe layer to decrease, the Fe layer is then divided into Fe particles with different diameters.(26) The annealed Fe surface works as the active catalyst to absorb the C_2H_2/H_2 gas into the particle. While the carbon atoms diffuse across the Fe particle to the opposite side, the self-organized nanotube with the hexagonal lattice is built vertically on the Si sample.(27) According to different fabrication methods, the electronic character of CNTs shows either metallic or semiconducting relying on the chirality with tube diameter or the grown condition.(3) Therefore, it reflects the importance of manufacture process in determining the electronic structure of CNTs and hence their applications.

Advanced applications of CNTs include chemical sensors,(7) nanoelectronic devices, (28) and field-emission devices.(29) In a field-emission experiment performed by Zhao *et al.*,(30) after UV or infrared light irradiation, as-grown CNTs sample showed an enhancement of emitted current and the decrease of its turn-on electric field. The possible reasons for the improved emission performance were attributed to the C-C bond breaking, structural damage, surface cleaning, or thermal effect. While the photon energy (PE) of incident light is larger than the energy of chemical bond (e.g. C-C bond = 6.29 eV, O-O bond = 5.16 eV, C-O bond = 3.2 eV, C-H bond = 3.5 eV),(31; 32) the bond breaking can occur by the photoelectron excitation effect. Even the covalent C-C bond insides CNTs has a chance to be broken if it allows the multi-photon excitation to happen. For example, Nd:YAG laser with PE of 4.66 eV is able to damage C-C bond, which results in the dangling bond.(30) Although the infrared light with PE by 1.18 eV can not break any chemical bond, it is observed the promotion in the performance of field-emission experiment. On the other hand, it can work well due to photothermal effect on the surface contamination.(33) These findings call for the detailed investigation of the mechanism that can account for the observed improvement in field emission results. Hence, it is worthwhile to probe the spatially-resolved electronic properties of CNTs after the treatment of laser trimming.

2.2 Chemical modification assisted by the focused laser technology

We introduce the He-Ne laser beam into the optical microscope for advanced application. Figure 1(a) and (b) show pictures of the optical microscope-focused laser beam system used in this work. Figure 1(b) emphasizes the scanning X-Y stage and objective lens in the optical microscope, which are essential for the creation of three-dimensional pattern using the focused laser beam. A schematic diagram of the set-up is shown in Figure 1(c). The He-Ne laser beam

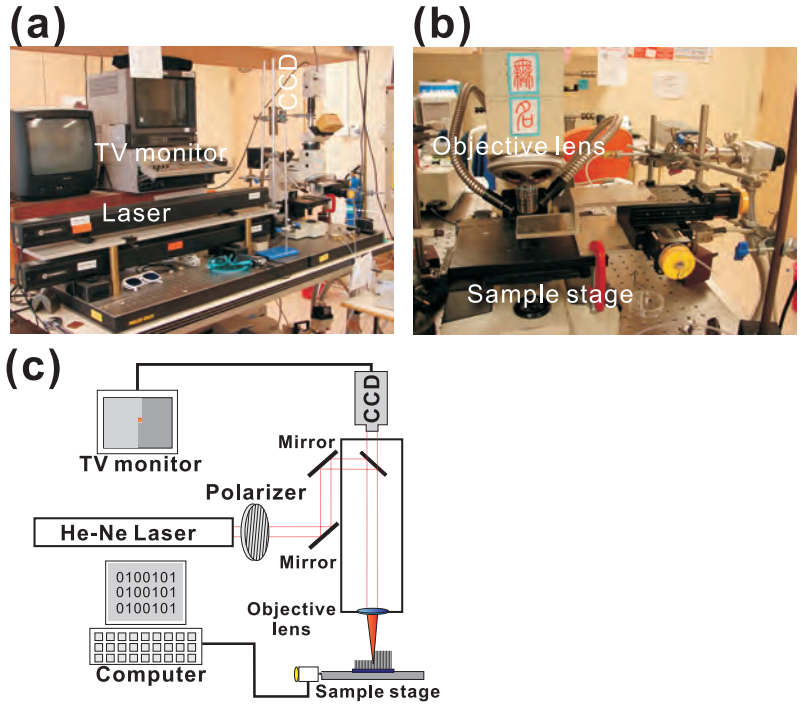

Fig. 1. (a)(b) Pictures of the optical microscope-focused laser beam system. (c) Outline of optical path inside the microscope and the computer-controlled pattern which is monitored by CCD simultaneously. The objective lens focusses the laser beam from a He-Ne laser (26 mW max) to a beam spot of $\sim 3\ \mu$m. The focused laser beam effectively trims away the CNTs and create a wide variety of micropatterns on the CNTs sample.

(632.8 nm) is directed into the optical microscope by controlling two reflecting mirrors. The beam splitter reflects the beam to the objective lens (magnification 50 $\times$) for focusing, and also allow the scattering light from the surface to be recorded. The optical image of laser-cutting pattern during laser incidence is simultaneously monitored by TV screen. Through the objective lens with a numberical aperture of 0.95, the laser beam is concentrated on its focal point with the micrometer size. The sample stage could adjust the z-axis position of the sample to bring the sample into focus. The computer-controlled X-Y stage offers an extensive capacity to form two-dimensional pattern or even three-dimensional structure of CNTs.(15) The laser beam through the tunable polarizer lens and mirrors is achieved to the maximum power of 26 mW.

In order to understand how gas molecule and morphological change affect the electronic structure of the CNTs, focused laser beam trimming of the CNTs can be conducted with the CNTs in vacuum or controlled gaseous environment. This was achieved with a transparent mini-chamber in the experiment that provides the vacuum and selective gaseous environments. Focused laser beam locally creates chemically active CNTs array, and allows the gaseous molecule to bond. By controlling the pressure and gas flow rate, the laser system could be operated with the sample housed in different gaseous environments.(15; 16)

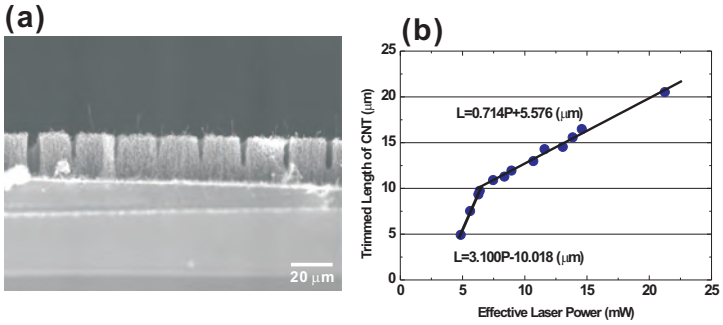

Fig. 2. (a) A cross-sectional SEM image of laser-trimmed CNTs. (b) Trimmed length of CNTs array as a function of laser power.

Therefore, the unique combination of gas cell environment with the focused laser allows us to probe the role of chemical bond inside CNTs.

3. Using laser beam to create activation sites in CNTs array

3.1 Different laser powers

Figure 2(a) shows the SEM image of CNTs array trimmed by different laser powers, which demonstrates the correlation between the laser power and the trimmed length of CNTs. The original CNTs array is about 20 μm in length. With the laser beam maintains the same focal point, the trimmed length of CNTs depends on the incident laser power. The laser power is precisely varied by a polarizer which is insected in the optical train of the laser beam as shown in Figure 1(c). Figure 2(b) exhibits the result of trimmed length as a function of laser power. The fitting result shows two linear equations separated at the transition point of 6.5 mW, although the detailed mechanism for such a transition is not clear at the moment. We believe that the untrimmed CNTs represent highly activated CNTs ready to form chemical functionalizaed species with the gaseous species inside the sample chamber. This is the origin of the excellent modification of electronic structure of CNTs array.

Figure 3(a) shows the cross-sectional SEM image of as-grown CNTs array before laser irradiation. Subsequently, the CNTs sample is irradiated by laser beam with different laser powers (7.8 mW, 10.8 mW, 15.0 mW, and 21.0 mW) in vacuum environment. Figure 3(b)$\sim$(e) reveal the laser impact on the residual part of CNTs array. The laser power of 7.8 mW ($>$ 3.1 mW minimum power) is capable of trimmed length at least 10 μm long. The morphology of the remaining CNTs after laser trimming exhibits an obvious increase in the diameter of nanotube on the top region of CNTs array. In Figure 3(c), while incident laser beam raises to the power by 10.8 mW, the tube size tends to get larger at the top region of CNTs array. It is believed that the injected laser beam causes the some parts of CNTs array to vanish, and its residual energy is available to be absorbd by CNTs array.

As the He-Ne laser offers the excited PE of only 1.96 eV, it is almost impossible to break C-C bond or C-O bond.(31) Hence, we believe the photothermal effect caused by laser beam shall dominate the trimming mechanism and its diameter-increased tendency. It causes the local annealing effect on its surface morphology and opens its structure for further modification. Meanwhile, the amount of laser-generated energy transport through the nanotubes is more than that dispersed inside the vacuum environment. It is observed that the larger power the

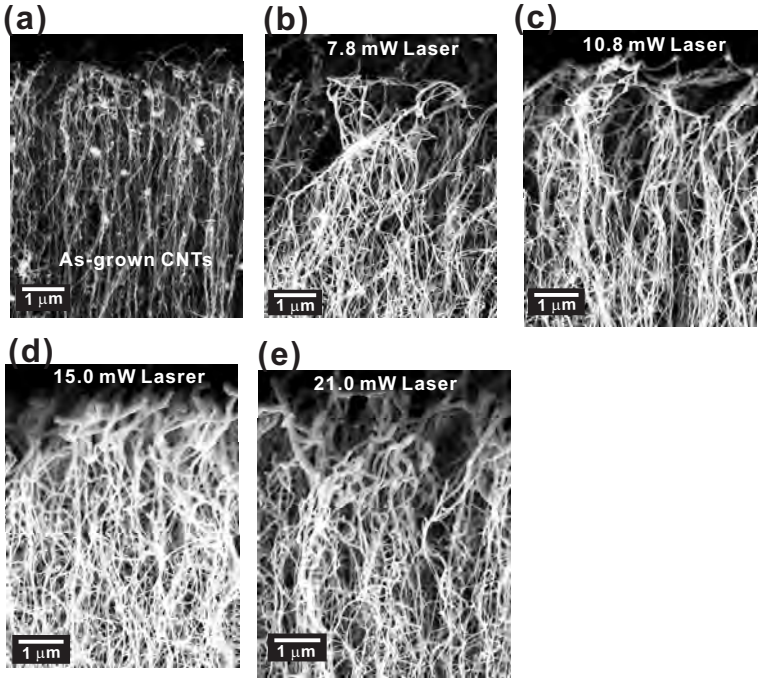

Fig. 3. (a) SEM image of as-grown CNTs. (b)∼(e) SEM images of modified CNTs with laser power of 7.8, 10.8, 15.0, and 21.0 mW, respectively.

laser beam imposes, the more enlarged diameter the segment of nantube shows. Although the major part of absorbed energy is able to make CNTs disappear by gas vaporization, the residual energy can make the tube size increase. The beginning of enlarged diameter should come from the structural reconstruction by the thermal melting effect. Previous study indicates that individual nanotube at annealing temperature of 1500 °C can coalesce a lot of nanotubes as a diameter-doubled tube.(34) It is apparent that the tube diameter at the bottom region is smaller than that at the top region. Therefore, the localized modification of lattice structure is exclusively found at the top region of CNTs array. It would be an advanced method to trim the morpholgy and tune its chemical performance reliably.

4. Spatially resolved chemical mapping of CNTs

4.1 Scanning PhotoElectron Microscopy (SPEM)

Owing to the powerful function of SPEM, it has been built at several synchrotron centers, e.g. NSRRC in Taiwan, PAL in South Korea, ALS in USA, and ELETTRA in Italy. In Taiwan, the SPEM is set at U5-SGM undulator beamline at NSRRC in Hsinchu. The photon energy of monochromatic X-ray could be operated from 60 to 1500 eV using a spherical grating monochromator (SGM).(20) The installed gratings (ruling density of 285, 400, 800, and 1600 l/mm) are used to provide the monochromator X-ray source. Due to the top-up mode of storage ring operated in NSRRC, the incident photon flux could maintain the same brightness during measurement. In Figure 4, the schematic describes the layout of U5 beamine and SPEM. The X-ray beam, which is collimated by the refocusing mirror and pinhole, overfill the

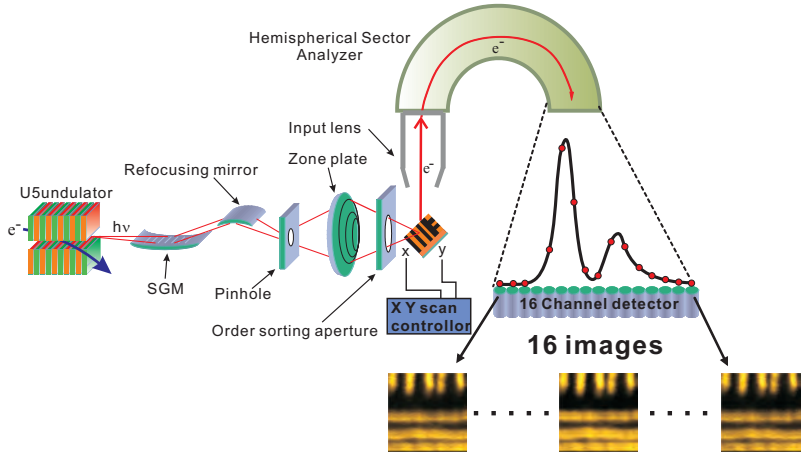

Fig. 4. Outline of SPEM equipment. The incident X-ray beam through the grating, refocusing mirror, and focusing optics is able to display the focused X-ray. The emitted photoelectron is acquired and collected by the 16-channel detector of HSA analyzer.

Fresnel zone plate (ZP) to produce the diffractive light. Order sorting aperture (OSA) behind the ZP could select the first-order diffractive beam for the purpose of given focusing X-ray. The spatial resolution and the focus length are ultimately dependent on the performance of ZP and OSA.(21) The optimal lateral resolution of X-ray beam is estimated about 100 nm.
Photoelectron excited by X-ray irradiation is collected by a 279.4-mm diameter hemispherical sector electron analyzer (HSA) with Omni V small-area lens and 16-channel detector (Physical Electronics). In order to acquire the maximum amount of photoelectrons, HSA with the acceptance angle of 7° is mounted at the angle of 54.7° with respect to the incident X-ray beam. This magic incident angle could receive a maximum intensity of photoelectrons due to the angular dependence of orbital angular symmetry. The 16-channel module using the same pass energy of HSA is capable of recording the energy distribution curve (EDC) of photoelectrons simultaneously. Adding the X-Y scanning function of flexure stage, SPEM could acquire a two-dimensional chemical image with 16 different BEs.(35; 36) The sample stage could be precisely probed at the certain location in the mapping image with the help of the readout device. The calibration of photon energy is measured from the 4f state of bulk Au sample or C 1s state of highly ordered pyrolytic graphite (HOPG) sample during the experiment.

4.2 Design of controllable gaseous environment insides laser-irradiatied CNTs system

As-grown CNTs are trimmed off by the focused laser in various gaseous environments (air, vacuum, N_2, and O_2). The modified morphology resembles the edge of sawtooth because the laser beam passes the focusing lens obliquely, as illustrated in Figure 5(a). As-grown and laser-modified area are manufactured together in one sample in order to study their respective electronic structure under the same experimental condition. Figure 5(b) shows the cross-sectional SEM image of modified CNTs. The inset of Figure 5(b) represents the magnified image of the sawtooth-shaped morphology. Figure 5(c) shows the C 1s SPEM image obtained by collecting photoelectrons of C 1s state. The top area of CNTs array, which genetrates the bright contrast, is dependent on the shadowing effect related to the acceptance angle of analyzer and highly intensive signal from the selected chemical state. Also, the

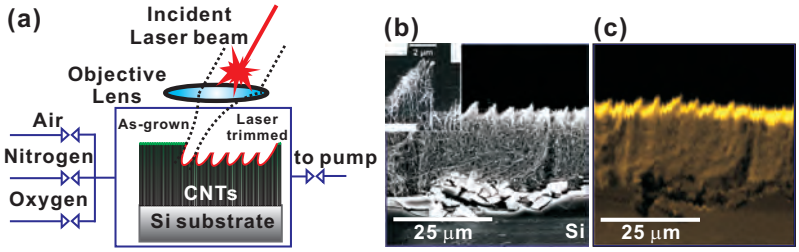

Fig. 5. (a) Schematic diagram of oblique focused laser beam to trim CNTs in the selected gaseous environment. (b)(c) Cross-sectional SEM image and corresponding SPEM image, respectively. The inset of (b) shows the magnified SEM image.

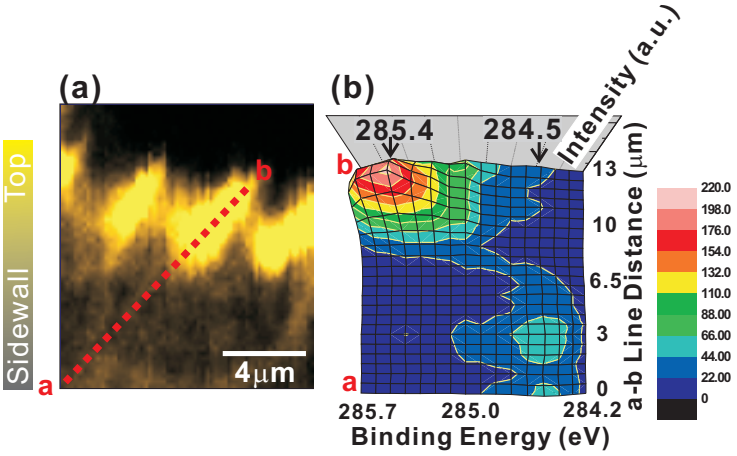

Fig. 6. (a) Cross-sectional SPEM image of laser-modified CNTs in air environment. The image corresponds to the intensity summation over 16 channels around C 1s state. (b) C 1s spectra taken along a-b line denoted in (a). The distance along a-b line is the ordinate and the binding energy of the 16-channel represents the abscissa. The colorimeter on the right side of (b) reflects the emission intensity of C 1s state collected from the individual channels. The chemical shift of 0.9 eV is observed between the laser-modified and sidewalls region.

intensity contrast on the sidewalls area is ascribed from the shadowing effect between the neighboring bundles. The cracks of the Si substrate in Figure 5(b)(c) clearly indicate that they are obtained from the same region of the sample.

5. Electronic structure evolution of laser-modified CNTs

5.1 Chemical shift of C 1s state of air-treated CNTs

Figure 6(a) shows a cross-sectional SPEM image of the laser-modified CNTs. The sample is treated in ambiance with laser power 19.3 mW. This mapping image stems from the intensity summation of the 16 SPEM images corresponding to the C 1s BE range between 284.2 and 285.7 eV. The C 1s spectra extracted along a-b line, as denoted in Figure 6(a), are analyzed to reveal its position-dependent electronic structures. These spectra are the intensity summation

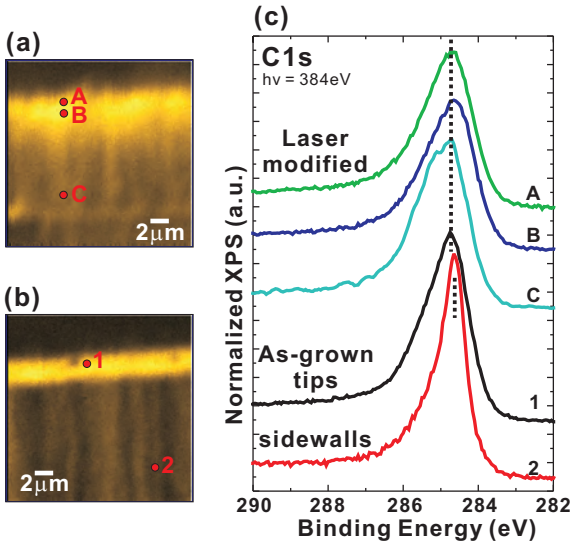

Fig. 7. (a) Cross-sectional SPEM C 1s image of CNTs for laser modification in vacuum. (b) Cross-sectional C 1s mapping image of as-grown CNTs. (c) Photoelectron spectra of C 1s state from as-grown area (position 1 and 2) and the area modified in vacuum (position A, B, and C).

over 400 nm $\times$ 400 nm square selected along a-b line. The shadowing effect can result in the higher signal intensity, instead of changing its EDC. Figure 6(b) reflects the 16-channel curves relative to C 1s state with 1.5 eV range. The ordinate is the position along the a-b line; abscissa is the BE of the 16 channels, the photoelectron intensity is represented by different colors. With the aid of this representative method, we can easily visualize the quantities of the spatially distributed chemical shifts with their relative intensity. Near the point "a" (around sidewalls region), the C 1s state shows the lowest BE with 284.5 eV, which is identical to the sidewalls of as-grown CNTs.(17) Around the point "b" (modified top region) the C 1s peak shifts to the highest BE with 285.4 eV. It is surprising that the chemical shift of C 1s state between sidewalls (a) and top (b) is as large as 0.9 eV. But in the pristine CNTs experiment,(18) the C 1s peak in the top region is higher than that in the sidewalls region only by 0.2 eV.

5.2 Role of coexisted gas molecule and laser assistance in chemical configuration of CNTs

As both adsorbed gas molecules and morphological change occur during laser irradiation, we design the vacuum experiment to clarify its correlation. Figure 7(a)(b) show the cross-sectional SPEM images, acquired around C 1s state with BE 282.5 $\sim$ 288.5 eV, with and without laser treatment in vacuum ($10^{-2} \sim 10^{-3}$ torr), respectively. Figure 7(c) shows the C 1s spectra of various locations denoted in Figure 7(a)(b). C 1s spectra obtained from the modified (A $\sim$ C) and as-grown top (1) areas show the same BE position. Compared to the spectrum measured at as-grown sidewalls area (2), it shows the slight up-shift of C 1s peak ($<$ 0.1 eV). The loss of gaseous molecule could reduce its possiblity of chemical reaction at the carbon site, while the laser beam breaks the covalent bond of hexagonal C-C structure. It means the morphological change alone is not sufficient to induce the up-shift of C 1s state, although it has ever been exposed to the air environment after laser irradiation.

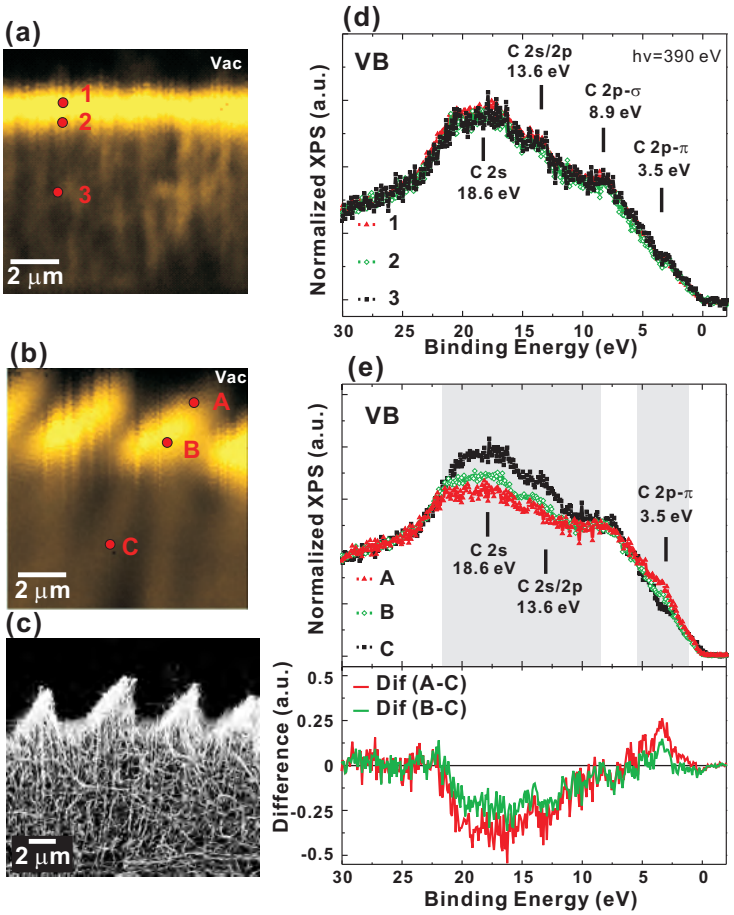

Fig. 8. (a)(d) Cross-sectional SPEM image of as-grown CNTs and air-treated CNTs, respectively. (b)(e) Spatially-resolved VB spectra from position 1 ∼ 3 of as-grown CNTs and position A ∼ C of air-treated CNTs. (c) SEM image relative to SPEM image of (b). The bottom figure of (e) provides the proof of DOS arrangement between 2p-π and 2p-σ electrons.

5.3 Rearrangment of DOS in air-treated CNTs

Figure 8(a) shows the cross-sectional SPEM image of as-grown CNTs, which is summarized by 16-channel images (C 1s BE 290.0 ∼ 278.0 eV). Figure 8(d) exhibits the position-relative VB spectra for the top region (1) and sidewalls region (2 and 3). The normalization process of VB spectra is critical for the density of state (DOS) comparison, thus the integrated intensity around BE 32.0 ∼ 31.0 eV is set to the same unity for the assumption of uniform scattering. The broad spectral feature around BE 18.6 eV is attributed to the formation of C 2s band, and the other feature around BE 13.6 eV is related to the mixing state of C 2s and C 2p band.(37) The C 2p-σ band of sp^2-hybridized carbon is identified around BE 8.9 eV, and the other C 2p-π band is assigned to BE 3.5 eV near to the Fermi edge.(38; 39)

As denoted "1" in Figure 8(a), the VB spectrum performs the DOS behavior where is near to the top of CNTs. While probing at the position 2 and 3, it shows the electronic behavior of sidewalls. The bright yellow area reflects more intensive signal of C 1s state from the top region (1) than the sidewalls region (2 and 3). The reason for the appearance of some stripes on the sidewalls area is the shadowing effect. According to the meaning of individual bands in VB spectra, we observe the similar DOS composition in the position $1 \sim 3$. In view of lattice structure, the close carbon cage at the end of nanotube involves the pentagon-related curvature and the dangling bond of unpaired π bond, which should make a change in the configuration of electronic structure. Thus, some groups have indicated that the uniquely structural characteristic at the tip stands for the DOS enhancement near the Fermi level.(17; 18) However, in our VB result we do not find any significant difference around BE $10.0 \sim 0$ eV between the top and sidewalls. That maybe result from different CNTs species or the sensitivity of probing positions around top region. The electronic performance between top and sidewalls rarely show any difference in C 2s, C 2s/2p, and C 2p-σ band. That is understood that the chemical binding mechanism happens to the outside electrons near Fermi level.

Figure 8(b)(c) show the cross-sectional SPEM and SEM image of trimmed CNTs. This sample is trimmed in ambient environment, as the same fabrication process in Figure 6(a). The sawtooth-shaped CNTs array results from the shift of incident axis of laser beam. The similar characteristic between chemical and morphological image manifests the ability to identify the spatially-resolved electronic structure. VB spectra, e.g. the position A and B for the top area and the position C for the sidewalls area, are exhibited in Figure 8(e). The bottom inset of Figure 8(e) is used to compare the spectral difference of top (A and B) and sidewalls (C). The adopted parameters for the experiments, i.e. incident X-ray angle, photon energy, and pass energy of HSA, are set to the same for comparsion. The VB performance measured at the position C in Figure 8(e) presents the same DOS distribution as that probed at top and sidewalls region of as-grown CNTs in Figure 8(d). VB spectra at position A and B appear more C 2p-π electrons between BE $5.2 \sim 2.1$ eV than that at the position C. Meanwhile, the spectral features around BE $21.0 \sim 9.0$ eV reflect the negative difference of A - C and B - C curve. Compared with the reference of sidewalls region (C), the transition from C 2s and C 2s/2p band to C 2p-π is observed at the irradiated top regions (A and B). This decreasing BE range including C 2s band and mixing C 2s/2p band accounts for the removal of carbon atoms or/and re-hybridization of DOS. The increasing DOS around C 2p-π state is ascribed to the production of structural defect with dangling bond or/and the gas hybridization effect. Because the unpaired π electron at the defect site behaves as the reactive site, the surrounding gas molecules could participate in its chemical hybridization. The transition of DOS in VB result is in agreement with the up-shift of C 1s state by 0.9 eV, which is given between the top and sidewalls region.

6. Variable chemical binding reactions

Laser-irradiated CNTs array in vacuum does not account for the direct correlation of the morphological change. Thus, high chemical shift in air-treated CNTs is attributed to the gas contribution involving the laser-induced reconstruction. In other words, the light irradiation is able to induce the chemical activity of sp^2-bonded carbon with the gas atom. In the sections below, we will discuss the N_2 and O_2-treated CNTs for the electronic modification and chemical functionalization.

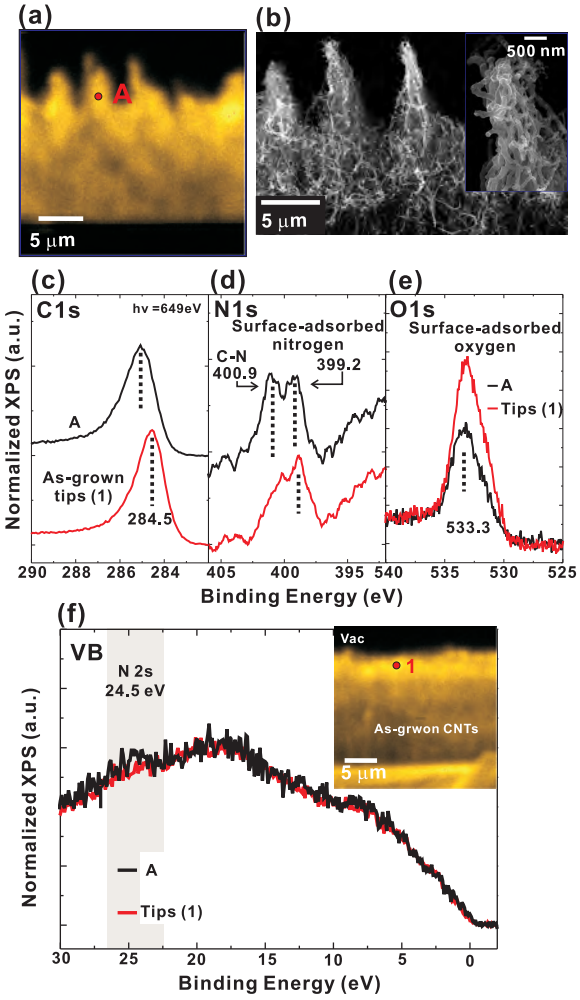

Fig. 9. (a)(b) Cross-sectional SPEM and SEM image of nitrogen-treated CNTs, respectively. The inset of (b) shows the morphology of laser-irradiated CNTs array. (c)-(f) Position-related C 1s, N 1s, O 1s and VB spectra. The inset of (f) shows the SPEM image of as-grown CNTs immersed in nitrogen environment. The sort of individual spectra, denoted A and as-grown tips, are used to compare its electronic change by laser exposure.

6.1 Nitrogen-treated CNTs

Figure 9(a)(b) present the SPEM and SEM image of the nitrogen-treated CNTs sample, respectively. The gas cell is filled with nitrogen gas (300 $\sim$ 500 torr) during the laser trimming process. The mapping image reveals the triangle shape of laser-trimmed CNTs similar to the morphology image taken by SEM. The high magnifcation SEM image as shown in the right corner of Figure 9(b) reveals the enlarged diameter of nanotubes, compared with the tube diameter in the sidewalls region. The position-resolved photoemission spectra (C 1s, N 1s,

O 1s, and VB), measured with photon energy by 649 eV, are exhibited in Figure 9(c) $\sim$ (f). The inset picture of Figure 9(f) shows the SPEM image of as-grown CNTs area, which is also transfered to the nitrogen-filled gas cell for comparsion. The character "A" and "1" on the top region of CNTs array are used to mark the position investigated by SPEM.

In Figure 9(c), C 1s spectrum obtained from the top region (poistion marked "A" in Fig. 9(a)) reveals the up-shift of C 1s state by 0.6 eV, as compared with as-grown CNTs (poistion marked "1" in inset of Fig. 9(f)). Figure 9(d) shows N 1s spectra with and without laser irradiation. The spectra have been smoothed without loss of energy resolution. The peak at 400.9 eV is related to C-N bond, the other one at 399.2 eV is ascribed to surface-adsorbed nitrogen(40) because both laser modified and as-grown areas have been immersed in nitrogen and ambiance environment. Two nitrogen peaks located at BE of 400.9 and 399.2 eV are found in the spectrum obtained after the CNTs has been irradiated by laser. Actually, the substitutional N atoms in the hexigonal carbon sheet could account for the up-shift of C 1s state and enhanced C-N bond (400.9 eV).(41)

It is also important to see the chemical reaction with oxygen species in N-treated CNTs, as shown in Figure 9(e). The oxygen feature at BE 533.3 eV is ascribed to the physically adsorbed oxygen molecule.(42) It makes sense that lower signal of physical oxygen absorption in the top region (A) is corresponding to the replacement action by C-N bond during laser irradiation.

In Figure 9(f), VB spectrum acquired from the top region of nitrogen-treated CNTs (A) shows the similar performance as that of the top region of as-grown CNTs (1), except for the spectral feature at BE 24.1 eV. It is assigned to N 2s band under the concession of C-N configuration.(43) However, the VB spectrum of as-grown CNTs (1) is quite different from the previous data of as-grown CNTs in Figure 8(b). It is found that VB spectra of the as-grown CNTs (1) after the nitrogen and ambient environment is quite sensitive to the surface contamination even without laser incidence. Surface-adsorbed features in N 1s state for the peak at BE 399.2 eV and in O 1s state for the peak of BE 533.2 eV are observed in both CNTs samples, which may determine the similar performance of VB spectra. In fact, due to enhanced C-N bond at BE 400.9 eV, the nitrogen-treated CNTs (A) reveals more intense feature in N 2s band than that of as-grown CNTs (1).

In short, the chemical shift of C 1s state by 0.6 eV is assigned to strong attachment of nitrogen gas, which is ascribed to the enhanced C-N bond in N 1s state. The surface-adsorbed nitrogen does not make the reorganization of C 1s state happen due to physical absorption. On the contrary, the DOS composition in VB spectra is very sensitive to the surface nitrogen contamination, which causes almost the same behavior. The DOS distribution with or without laser irradiation does not exhibit the difference. In terms of the existence of C-N bond, it is obtained that N 2s band in VB specteum is slight enhanced by laser irradiation.

6.2 Oxygen-treated CNTs

Since nitrogen-treated CNTs have shown the possibility to modify chemical property, the introduction of oxygen gas is the alternative route for engineering the electronic structure effectively. CNTs sample is irradiated by laser beam with laser power of 14.8 mW within oxygen environment (300 $\sim$ 600 torr). As-grown CNTs, existed on the rest of laser-irradiated sample, are exposed to the same oxygen environment and ambient transport process, too. Figure 10(a)(b) reveal the SPEM and SEM image of oxygen-treated CNTs, respectively. The inset of Figure 10(b) highlights some melting balls and fusion of nanotube bundles after laser irradiation. Figure 10(c)(d)(e) exhibit C 1s, O 1s, and VB spectra for the individual positions of oxygen-treated (position "B" and "C" marked in Fig. 10(a)) and as-grown (position marked "2"

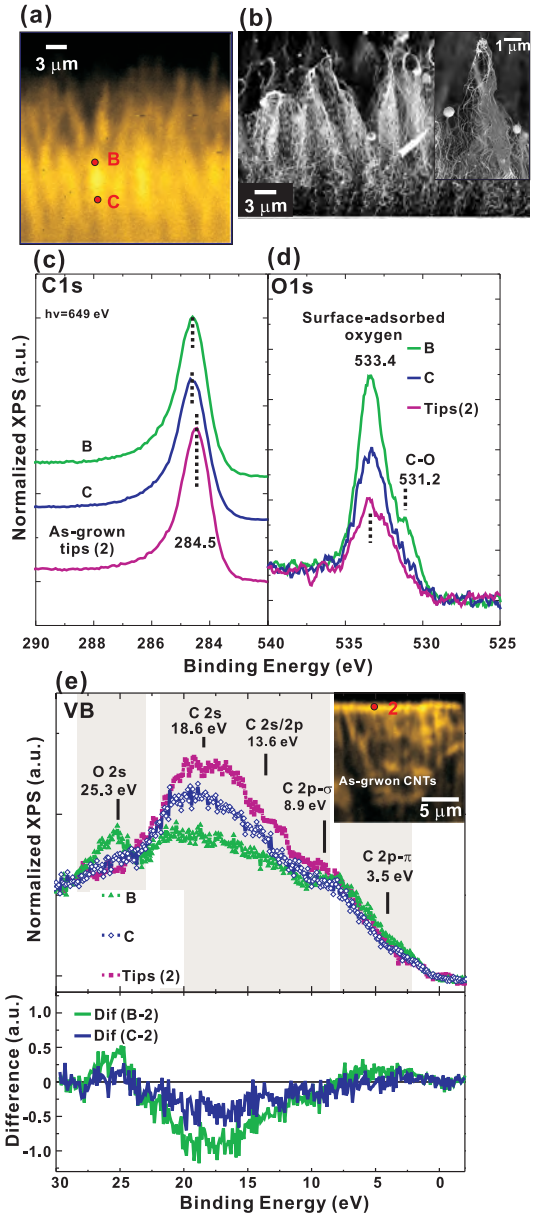

Fig. 10. (a)(b) SPEM and SEM images of oxygen-treated CNTs, respectively. The inset of (b) magnifies the laser-irradiated morphology, which suffered from local heating dose and oxygen gas. (c)∼(e) Position-related C 1s, N 1s, and VB spectra. The inset of (e) shows the SPEM image of as-grown CNTs without the laser irradiation. Difference between as-grown and laser-irradiated spectra demonstrates the modification of DOS in VB range, as shown in the bottom figure of (e).

in inset of Fig. 10(e)) CNTs. The measured positions are also marked in the mapping image of Figure 10(a) and the inset of Figure 10(e).
In Figure 10(c), the C 1s peak (B and C) after laser irradiation shifts toward higher BE, however only by 0.2 eV relative to the top region of as-grown CNTs (position "2"). In Figure 10(d) O 1s spectrum (B) exhibits two oxidation states located at BE 533.4 and 531.2 eV. The weak feature at BE 531.2 eV is related to C-O bond, and the other feature at BE 533.4 eV is ascribed to the adsorbed oxygen linked to carbon.(42) Physically adsorbed oxidation is also seen in N-treated CNTs (Figure 9(e)), because of the ambient transport process. The intensity of C-O bond at the top region (B) is larger than that near sidewalls (C), due to the energy localization. Meanwhile, the amounts of adsorbed oxygen at the modified regions (B and C) are more than that top region of as-grown CNTs (2), individually. It is considered that opening the tubular network of CNTs is possbile to add the buliding site of C-O bond and has the side effect to enhance surface-adsorbed oxygen.
VB spectra of as-grown area (2) and oxygen-treated area (B and C) are illustrated in Figure 10(e). The bottom part of Figure 10(e) is the spectral difference between oxygen-treated (B and C) and as-grown area (2). It is found that the broad range between BE 22.1 $\sim$ 8.0 eV in the oxygen-treated CNTs (B and C) shows the decreasing tendency compared with the reference spectrum of as-grown area (2). This spectral range includes the C 2s band at BE 18.6 eV, mixing C 2s/2p band at BE 13.6 eV, and C 2p-σ band at BE 3.5 eV. Apparently, the change between "B" and "2" is larger than that between "C" and "2", becuase of the rearrangement of DOS and morphological change. The C 2p-π band around BE 3.5 eV close to Fermi level presents the slight enhancement at the top region of oxygen-treated CNTs (B), but at the sidewalls region (C) it does not. Dangling bond and defect site may result in the increasing intensity of 2p-π band after laser irradiation. Indeed, the O 2s-derived band at BE 25.3 eV is obviously raised in the oxygen-treated CNTs (B). By contrast, the resultant spectrum of the sidewalls region (C) appears less enhanced around O 2s-derived band. The appearance of C-O state in O 1s state and O 2s band in VB spectrum could count on the formation of C-O chemical bond.
The surface-adsorbed oxygen feature at BE 533.4 eV demonstrates the intensity enhancement from the position of sidewalls region (C) to top region (B). It seems that laser impact generates the structural defect and the activity site to bond oxygen atom. Therefore, the physisorbed oxygen amount on the surface should be induced by the influence of laser irradiation. The removal of carbon atoms and oxygen contamination may result in the decreasing intensity and re-hybridization around C 2s and C 2s/2p band (BE 22.1 eV $\sim$ 8.0 eV). Meanwhile, C 2p-π band around BE 8.0 $\sim$ 2.0 eV is increased while the C-O chemical bond occurs, in particular the case of top region (B). In fact, the formation of chemical C-O state increases the extra factor inside the DOS re-distribution; therefore, without this, like the case of the sidewalls region (C), it shows the middle modification due to the less impact of dangling bond and chemical C-O bond.(44; 45) The structural defect and dangling bond of CNTs after laser trimming should be the important factors in the DOS reconstruction.(46) It means the eliminated amount of C 2s and C 2s/2p band and increased C 2p-π intensity is in agreement to the result of air-treated CNTs. In fact, the behavior of C 2p-π electrons of oxygen-treated CNTs is observed for a little different, because the mixing contribution between air environment and laser-induced defect play the important role in C 2p-π electrons.

7. Discussion

The dangling bonds and topological defects are supposed to be increased upon laser trimming.(29) Naturally, laser trimming causes the breakage of the C-C bond in CNTs and

the gas molecules nearby can bond to the C atoms possessing dangling bonds. The existence of stable C-N and C-O bonds on the surface of nanotubes was expected to become metallic, independent of the tubular diameter and chirality.(7; 47) Both N_2 and O_2 molecules can be bonded with CNTs assisted by laser and result in the different chemical shifts (0.6 and 0.2 eV). The highest chemical shift (0.9 eV) in the air-treated CNTs may be attributed to the mixing gas contribution, which needs to be further studied. On the other hand, the result of vacuum-treated CNTs shows the slight up-shift of C 1s state (< 0.1 eV). However, even after the gas treatment, a lot of defects are still expected to exist at the laser trimmed surface of the gas-treated CNTs. These defects may also contribute to the observed C 1s chemical shift besides the gas interaction. A shift of C 1s state is observed at higher BE shoulder as a result of the reconstruction of chemical environment between the structural defect and gas atom.

In terms of VB spectra, the air-treated CNTs yields the local modification of DOS at the top region of CNTs array, where results in the raising C 2p-π electron and decreasing C 2s and C 2p-σ electron. After studying the influence of gaseous environments on laser trimming of CNTs, the laser irradiation plus oxygen contribution dominate the reorganization of DOS. The DOS change between π and σ band is corresponding to the existence of C-O bond and generation of structural defect. Furthermore, the surface-adsorbed contamination of N_2 molecules can largely influence the DOS distribution. While we consider the laser-induced defect and dangling bond after laser irradiation, the bonded gas molecules at the defective sites are both available at the trimmed surface. This kind of combination causes the obvious modification of DOS distribution in VB.

Hence, the dangling bond of defective site and gas contamination shall take the essential contribution of the reconstruction of DOS. It is believed that laser irradiation is a viable technique for functionalizing CNTs incorporating with N and O atoms. By controlling the type of gas molecules used, we can change and tune the electronic character of CNTs for the development of electronic device. Laser technology provide the stage of localized chemical modification for the novel applications.

8. Acknowledgement

Authors greatly acknowledge the support and fruitful discussion of Dr. Chia-Hao Chen, Dr. Yanwu Zhu, Prof. Shangjr Gwo, Prof. Shien-Der Tzeng, Dr. Yin-Ming Chang, Mr. Chih-Wei Peng, Mr. Sheng-Syun Wong, Mr. Po-Tsong Wu, and Ms. Soi-Chan Lei. This work was supported by the National Science Council of Taiwan under grant no. NSC 98-2120-M-002-010.

9. References

[1] Iijima, S. (1991). Helical Microtubules of Graphitic Carbon. *Nature*, Vol. 354, pp. 56-58, Doi:10.1038/354056a0

[2] Thess, A.; Lee, R.; Nikolaev, P.; Dai, H.; Petit, P.; Robert, J.; Xu, C.; Lee, Y. H.; Kim, S. G.; Rinzler, A. G.; Colbert, D. T.; Scuseria, G. E.; Tomanek, D.; Fischer, J. E. & Smalley, R. E. (1996). Crystalline Ropes of Metallic Carbon Nanotubes. *Science*, Vol. 273, pp. 483-487. Doi:10.1126/science.273.5274.483

[3] Wildöer, J. W. G.; Venema, L. C.; Rinzler, A. G.; Smalley, R. E. & Dekker C. (1998). Electronic Structure of Atomically Resolved Carbon Nanotubes. *Nature*, Vol. 391, pp. 59-62. Doi:10.1038/34139

[4] Hamada, N.; Sawada, S. & Oshiyama, A. (1992). New One-dimensional Conductors: Graphitic Microtubules. *Phys. Rev. Lett.*, Vol. 68, pp. 1579-1581. Doi:10.1103/PhysRevLett.68.1579

[5] Demczyk, B. G.; Wang Y. M.; Cumings J.; Hetman, M.; Han, W.; Zettl, A. & Ritchie, R. O. (2002). Direct Mechanical Measurement of the Tensile Strength and Elastic Modulus of Multiwalled Carbon Nanotubes. *Mater. Sci. Eng. A*, Vol. 334, pp. 173-178. Doi: 10.1016/S0921-5093(01)01807-X

[6] Dai, H. J.; Hafner, J. H.; Rinzler, A. G.; Colbert, D. T. & Smalley, R. E. (1996). Direct Mechanical Measurement of the Tensile Strength and Elastic Modulus of Multiwalled Carbon Nanotubes. *Nature*, Vol. 384, pp. 147-150. Doi:10.1038/384147a0

[7] Collins, P. G.; Bradley, K.; Ishigami, M.; & Zettl, A (2000). Extreme Oxygen Sensitivity of Electronic Properties of Carbon Nanotubes. *Science* Vol. 287, pp. 1801-1804. Doi: 10.1126/science. 287.5459.1801

[8] Yoo, E.; Gao, L.; Komatsu, T.; Yagai, N.; Arai, K.; Yamazaki, T.; Matsuishi, K.; Matsumoto, T.; & Nakamura J. (2004). Atomic Hydrogen Storage in Carbon Nanotubes Promoted by Metal Catalysts. *J. Phys. Chem. B*, Vol. 108, No. 49, pp. 18903-18907. Doi: 10.1021/jp047056q

[9] Berber, S.; Kwon, Y. K.; & Tomanek D. (2000). Unusually High Thermal Conductivity of Carbon Nanotubes. *Phys. Rev. Lett.*, Vol. 84, pp. 4613-4616. Doi: 10.1103/PhysRevLett.84.4613

[10] Klein, K. L., Melechko, A. V.; McKnight, T. E.; Retterer, S. T.; Rack, P. D.; Fowlkes, J. D.; Joy, D. C.& Simpson, M. L. (2008). Surface Characterization and Functionalization of Carbon Nanofibers. *J. Appl. Phys.*, Vol. 103, pp. 061301-061327. Doi:10.1063/1.2840049

[11] Peng, S. & Cho, K. (2000). Chemical Control of Nanotube Electronics. *Nanotechnology*, Vol. 11, pp. 57-60. Doi: 10.1088/0957-4484/11/2/303

[12] Gohel, A.; Chin, K. C.; Zhu, Y. M.; Sow, C. H.; & Wee, A. T. S. (2005). Field Emission Properties of N_2 and Ar Plasma-treated Multi-wall Carbon Nanotubes. *Carbon*, Vol. 43, pp. 2530-2535.

[13] Lee, H. J.; Lee, Y.D.; Moon, S. I.; Cho, W. S.; Lee, Y. H.; Kim, J. K.; Hwang, S. W.; & Ju, B. K. (2000). Enhanced Surface morphologies of Screen-printed Carbon Nanotube Films by Heat Treatment and Their Field-emission Properties. *Carbon*, Vol. 44, pp. 2625-2630.

[14] Saurakhiya, N.; Zhu, Y. W.; Cheong, F. C.; Ong, C. K.; Wee, A. T. S.; Lin, J. Y.; & Sow, C. H. (2005). Pulased Laser Deposition-assisted Patterning of Aligned Carbon Nanotubes Modified by Focused Laser Beam for Efficient Field Emission. *Carbon*, Vol. 43, pp. 2128-2133.

[15] Lim, K. Y.; Sow, C. H.; Lin, J.; Cheong, F. C.; Shen, Z. X.; Thong, J. T. L.; Chin, K. C. & Wee, A. T. S., (2003). Laser Pruning of Carbon Nanotubes as a Route to Static and Movable Structures. *Adv. Mater.*, Vol. 15, pp. 300-303. Doi: 10.1002/adma.200390072

[16] Cheong, F. C.; Lim, K. Y.; Sow, C. H.; Lin, J.; & Ong, C. K. (2003). Large Area Patterned Arrays of Aligned Carbon Nanotubes via Laser Trimming. *Nanotechnology*, Vol. 14, No. 4, pp. 433-437. Doi: 10.1088/0957-4484/14/4/305

[17] Suzuki, S.; Watanabe, Y.; Ogino, T.; Heun, S.; Gregoratti, L.; Barinov, A.; Kaulich, B.; Kiskinova, M.; Zhu, W.; Bower C. & Zhou, O. (2002) Electronic Structure of Carbon Nanotubes Studied by Photoelectron Spectromicroscopy. *Phys. Rev. B*, Vol. 66, pp. 035414. Doi: 10.1103/PhysRevB.66.035414

[18] Chiou, J. W.; Yueh, C. L.; Jan, J. C.; Tsai, H. M.; Pong, W. F.; Hong, I. H.; Klauser, R.; Tsai, M. H.; Chang, Y. K.; Chen, Y. Y.; Wu, C. T.; Chen, K. H.; Wei, S. L.; Wen, C. Y.; Chen,

l. C.; & Chuang, T. J. (2002). Electronic Structure of the Carbon Nanotube Tips Studied by X-ray-absorption Spectroscopy and Scanning Photoelectron Microscopy. *Appl. Phys. Lett.* Vol. 81, pp. 4189-4192. Doi:10.1063/1.1523152

[19] de Heer, W. A.; Châtelain, A.& Ugarte D., (1995). A Carbon Nanotube Field-Emission Electron Source. *Science*, Vol. 270, No. 5239, pp. 1179-1180. Doi:10.1126/science.270.5239.1179

[20] Hong, I. H.; Lee, T. H.; Yin, G. C.; Wei, D. H.; Juang, J. M.; Dann, T. E.; Klauser, R.; Chuang, T. J.; Chen, C. T.; & Tsang, K. L., (2001). Performance of the SRRC Scanning Photoelectron Microscope. *Methods Phys. Res. A*, Vol. 467-468, pp. 905-908.

[21] Klauser, R.; Hong, I. H.; Lee, T. H.; Yin, G. C.; Wei, D. H.; Tsang, K. L.; Chuang, T. J.; Wang, S. C.; Gwo, S. & Zharnikov, M. (2001). Zone-plate-based Scanning Photoelectron Microscopy at SRRC: Performance and Applications. *Surface Review and Letters*, Vol. 9, No. 1, pp. 213-222.

[22] Journet, C.; Maser, W. K.; Bernier, P.; Loiseau, A.; de la Chappelle, M. L.; Lefrant, S.; Deniard, P.; Lee, R. & Fischer, J. E. (1997). Large-scale Production of Single-walled Carbon Nanotubes by the Electric-arc Technique. *Nature*, Vol. 388, pp. 756-758.

[23] Thess, A.; Lee, R.; Nikolaev, P.; Dai, H. J.; Petit, P.; Robert, J.; Xu, C. H.; Lee, Y. H.; Kim, S. G.; Rinzler, A. G.; Colbert, D. T.; Scuseria, G. E.; Tomanek, D.; Fischer, J. E. & Smalley R. E. (1996). Crystalline Ropes of Metallic Carbon Nanotubes. *Science*, Vol. 273, pp. 483. Doi:10.1126/science.273.5274.483

[24] Iijima, S. & Ichihashi, T. (1993). Single-shell Carbon Nanotubes of 1-nm Diameter. *Nature*, Vol. 363, pp. 603-605. Doi:10.1038/363603a0

[25] Wang, Y. H.; Lin, J.; Huan, C. H. A. & Chen, G. S. (2001). Synthesis of Large Area Aligned Carbon Nanotube Arrays from C_2H_2 - H_2 Mixture by rf Plasma-enhanced Chemical Vapor Deposition. *Appl. Phys. Lett.*, Vol. 79, pp.680-682. Doi:10.1063/1.1390314

[26] Chhowalla, M.; Teo, K. B. K.; Ducati, C.; Rupesinghe, N. L.; Amaratunga, G. A. J.; Ferrari, A. C.; Roy, D.; Robertson, J. & Milne, W. I. (2001). Growth Process Conditions of Vertically Aligned Carbon Nanotubes Using Plasma Enhanced Chemical Vapor Deposition. *J. Appl. Phys.*, Vol. 90, pp. 5308-5317. Doi:10.1063/1.1410322

[27] Fan, S.; Chapline, M. G.; Franklin, N. R.; Tombler, T. W.; Cassell, A. M. & Dai, H. (1999). Self-oriented Regular Arrays of Carbon Nanotubes and Their Field Emission Properties. *Science*, Vol. 283, pp. 512-514. Doi:10.1126/science.283.5401.512

[28] Collins, P. G.; Arnold, M. S. & Avouris, P. (2001). Engineering Carbon Nanotubes and Nanotube Circuits Using Electrical Breakdown. *Science*, Vol. 292, pp. 706-709. DOI:10.1126/science.1058782

[29] Rinzler, A. G.; Hafner, J. H.; Nikolaev, P.; Lou, L.; Kim, S. G.; Tománek, D.;Nordlander, P.; Colbert, D. T. & Smalley, R. E. (1995). Unraveling Nanotubes: Field Emission from an Atomic Wire. *Science*, Vol. 269, pp. 1550-1553. Doi:10.1126/science.269.5230.1550

[30] Zhao, W. J.; Kawakami, N.; Sawada, A. & Takai, M. (2003). Field Emission from Screen-printed Carbon Nanotubes Irradiated by Tunable Ultraviolet Laser in Different Atmospheres. *J. Vac. Sci. Technol. B*, Vol. 21, pp. 1734-1737. Doi:10.1116/1.1587136

[31] Yavas, O.; Suzuki, N.; Takai, M.; Hosono, A. & Kawabuchi, S. (1998). Laser Cleaning of Field Emitter Arrays for Enhanced Electron Emission. *Appl. Phys. Lett.*, Vol. 72, pp. 2797-2780. Doi:10.1063/1.121461

[32] Rochanachirapar, W.; Murakami, K.; Yamasaki, N.; Abo, A.; Wakaya, F.& Takai, M. (2005). Influence of Gas Atmosphere during Laser Surface Treatment of CNT Cathode. *J. Vac. Sci. Technol. B*, Vol.23, pp.762-765. Doi:10.1116/1.1868698

[33] Hwang, J. D.; Chen, k. F.; Chan, L. H. & Chang, Y. Y. (2006). Using Infrared Laser to Enhance Field Emission of Carbon Nanotube. *Appl. Phys. Lett.*, Vol. 89, pp. 33103-33106. Doi:10.1063/1.2222337

[34] Nikolaev, P.; Thess, A.; Rinzler, A. G.; Colbert, D. T. & Smalley, R. E. (1997). Diameter Doubling of Single-wall Nanotubes. *Chem. Phys. Lett.*, Vol. 266, pp. 422-426.

[35] Chuang, C. H.; Chen, C. H.; Chang, Y. M.; Peng, C. W.; Wong, S. S.; Tzeng, S. D.; Gwo, S.; Zhu, Y.; Sow, C. H. & Lin, M. T. (2007). Enhanced Chemical Shift of Carbon Nanotube from Laser Assisted Gas Incorporation. *Appl. Phys. Lett.*, Vol. 91, pp. 183101. Doi:10.1063/1.2801698

[36] Klauser, R., Hong, I. H.; Su, H. J.; Chen, T. T.; Gwo, S.; Wang, S. C.; Chuang, T. J. & Gritsenko, V. A.(2001). Oxidation States in Scanning-probe-induced Si_3N_4 to SiO_x Conversion Studied by Scanning Photoemission Microscopy. *Appl. Phys. Lett*, Vol. 79, pp. 3143-3145. Doi:10.1063/1.1415415

[37] Larciprete, R.; Goldoni, A.; Lizzit, S.& Petaccia, L. (2005). The Electronic Properties of Carbon Nanotubes Studied by High Resolution Photoemission Spectroscopy. *Appl. Sur. Sci.*, Vol. 248, pp. 8-13. doi:10.1016/j.apsusc.2005.03.023

[38] Schiessling, J.; Kjeldgaard, L.; Rohmund, F.; Falk, L. K. L.; Campbell, E. E. B.; Nordgren, J. & Brühwiler, P. A. (2003). Synchrotron Radiation Study of the Electronic Structure of Multiwalled Carbon Nanotubes. *J. Phys.: Condens. Matter*, Vol. 15, pp.6563-6579. Doi: 10.1088/0953-8984/15/38/022

[39] Bianconi, A.; Hagström, S. B. M. & Bachrach, R. Z. (1977). Photoemission Studies of Graphite High-energy Conduction-band and Valence-band States using Soft-x-ray Synchrotron Radiation Excitation. *Phys. Rev. B*, Vol. 16, pp. 5543-5548. Doi:10.1103/PhysRevB.16.5543

[40] Kim, T. Y.; Lee, K. R.; Eun, K. Y.; Oh, K. H.; Carbon Nanotube Growth Enhanced by Nitrogen Incorporation. *Chem. Phys. Let.*, Vol. 372, pp. 603-607.

[41] Lim, S. H.; Elim, H. I.; Gao, X. Y.; Wee, A. T. S.; Ji, W.; Lee j. Y. & Lin, J. (2006). Electronic and Optical Properties of Nitrogen-doped Multiwalled Carbon Nanotubes. *Phys. Rev. B*, Vol. 73, pp. 045402. Doi:10.1103/PhysRevB.73.045402

[42] Valentini, L.; Lozzi, l.; Picozzi, S.; Cantalini, C.; Santucci, S. & Kenny, J.M. (2004). Adsorption of Oxidizing Gases on Multiwalled Carbon Nanotubes. *J. Vac. Sci. Technol. A*, Vol. 22, pp. 1450. Doi:10.1116/1.1705588

[43] Ray, S. C.; Pao, C. W.; Tsai, H. M.; Chiou, J. W.; Pong, W. F.; Chen, C. W.; Tsai, M. H.; Papakonstantinou, P.; Chen, L. C. & Chen, K. H. (2007). A Comparative Study of the Electronic Structures of Oxygen- and Chlorine-treated Nitrogenated Carbon Nanotubes by X-ray Absorption and Scanning Photoelectron Microscopy. *Appl. Phys. Lett.*, Vol.91, pp. 202102. Doi:10.1063/1.2807275

[44] Bittencourt, C.; Felten, A.; Douhard, B.; Ghijsen, J.; Johnson, R. L; Drube, W. & Pireaux, J. J. (2006). Photoemission Studies of Gold Clusters Thermally Evaporated on Multiwall Carbon Nanotubes. *Chem. Phys.*, Vol. 328, pp. 385-391. Doi:10.1016/j.chemphys.2006.07.041

[45] Lim, S. C.; Jo, C. S.; Jeong, H. J.; Shin, Y. M.; Lee, Y. H.; Samayoa, I. A.; & Choi, J. (2002). Effect of Oxidation on Electronic and Geometric Properties of Carbon Nanotubes. *Jpn. J. Appl. Phys.*, Vol.41, No. 9, pp. 5635-5639. Doi: 10.1143/JJAP.41.5635

[46] Belavin, V. V.; Bulusheva, L. G. & Okotrub, A. V. (2004). Modifications to the Electronic Structure of Carbon Nanotubes with Symmetric and Random Vacancies. *Int. J. Quantum Chem.*, Vol. 96, pp. 239-246. Doi: 10.1002/qua.10629

[47] Miyamoto, Y.; Cohen, M. L. & Louie, S. G. (1997). Theoretical Investigation of Graphitic Carbon Nitride and Possible Tubule Forms. *Solid State Commun.* Vol.102, pp. 605-608. Doi:10.1016/S0038-1098(97)00025-2